Communications in Computational Chemistry
Commun. Comput. Chem., Vol. 7, No. 3, 264–273
doi: 10.4208/cicc.2025.120.01

Regular Article

Machine Learning Force Fields for Predicting Thermodynamic Properties of PA6T/6I Copolymers

Yingwei Xie[1], Lele Wei[1] and Jin Wen[1,*]

[1]*State Key Laboratory of Advanced Fiber Materials, College of Materials Science and Engineering, Donghua University, Shanghai 201620, China.*

[*] Corresponding authors: jinwen@dhu.edu.cn

Received on 30 April 2025; Accepted on 4 June 2025

Abstract: This study employed molecular dynamics (MD) simulations, utilizing both a machine learning force field (MACE-OFF) and a traditional force field (PCFF), to predict the thermal properties of poly(hexamethylene terephthalamide-co-isophthalamide) (PA6T/6I) copolymers. The simulations are benchmarked against experimental data to assess the predictive accuracy of these two methodologies for the thermal properties of PA6T/6I copolymers. Our findings reveal that the MACE-OFF force field, after calibration for the PA6T/6I copolymer, offers significant precision in modeling π-π and hydrogen-bonding interactions, closely mirroring the results from M06 functional simulations. The MD simulations underscore the MACE-OFF model's ability to deliver more stable thermal properties, including the glass transition temperature (T_g) and density, for copolymer systems with varying PA6T content, aligning well with experimental observations. Furthermore, a comprehensive analysis of dynamic properties, such as mean squared displacement and free volume, within the PA6T/6I copolymers was performed to decipher the mechanisms underlying the temperature-dependent changes in thermal properties observed throughout the simulation process. A thorough examination of the fluctuations in inter-chain and intra-chain hydrogen bonding within the copolymer systems has unveiled the correlation between the molecular packing arrangement and thermal properties. This research establishes that the MACE-OFF model accurately simulates the thermal dynamical behavior of PA6T/6I copolymers, a capability that could be extended to other polyamide systems.

Key words: machine learning, force field, molecular dynamics simulations, Poly(hexamethylene terephthalamide-co-isophthalamide) (PA6T/6I) copolymers, thermal properties

1. Introduction

Simulating the thermal properties of polymers necessitates an understanding of their microstructures, which is challenging due to the intricate conformations of polymers and the time-consuming nature of such predictions. Hence, selecting an appropriate method for polymer dynamics simulations is crucial for accurately predicting polymer properties. Although ab initio molecular dynamics (AIMD) methods [1,2], which employ density functional theory (DFT) [3], offer highly accurate depictions of the electronic structure and enable precise capturing of intermolecular interactions, they are restricted to small systems with relatively short timescales and are computationally intensive. Consequently, their application to complex systems like polymers is problematic [4,5]. As a result, classical molecular dynamics (MD) simulations are frequently utilized for large-scale polymer computations.[6] However, traditional MD simulations depend on empirically derived potential functions, which can compromise the accuracy of the simulations [7]. Therefore, there is a pressing need to develop efficient methods that balance precision and computational efficiency in polymer dynamics simulations.

In recent years, the advent of machine learning techniques, particularly machine learning force fields (MLFF) [8-12], has presented a promising solution for the precise study of polymer MD. Machine learning potentials learn nonlinear functional relationships from extensive datasets of structural samples and their corresponding property outputs, akin to an effective set of quantum mechanical potential rules [13], thus circumventing the need to directly solve the complex and elusive physical relationships between sample structures and their properties. One of the early algorithms associated with machine learning is the feedforward

neural network [14]. However, this approach lacks a clear feature selection mechanism and is limited in its capacity to represent complex molecular structures and interactions. For instance, Teso-Fz-Betoño et al. encountered issues such as vanishing gradients and contradictory gradient directions when training with feedforward networks [15]. The Behler-Parrinello neural network (BPNN) method [16] can handle the spatial positions of all atoms in a system, thereby predicting the total energy and forces. Vassilev-Galindo et al. applied the BPNN model to predict the thermal isomerization process of azobenzene and found that BPNN is overly reliant on local descriptors, which hinders its ability to effectively capture long-range interactions [17]. This limitation leads to suboptimal performance when dealing with larger or more complex flexible molecules [17]. The message passing neural network (MPNN) [18,19] is a neural network architecture designed for graph-structured data, learning the representation of the graph through a message-passing mechanism between nodes and edges. Xue et al. combined MPNN with ReaxFF, using MPNN to compute bond order and bond energy, thereby enhancing the performance in calculating the potential energy surface, reaction energies, and equation of state.[20] However, most MPNN-based interatomic potentials use message passing that only considers two-body interactions, which may pose challenges to the generalizability of the model [21].

Due to the issues mentioned above, finding a suitable model framework for MD simulations is particularly important. The MACE model [22], based on an equivariant graph neural network architecture, is characterized by its use of a high-order many-body message passing mechanism, which enables high-precision predictions with very few message passing iterations. Grunert et al. were able to accurately predict properties such as activation energy in MD processes and significantly improve accuracy through simple fine-tuning [23]. The model trained with MACE demonstrated high accuracy in bond dissociation predictions and exhibited strong extrapolation capabilities, enabling predictions for non-equilibrium structures [24]. In summary, the MACE model has demonstrated high accuracy and excellent extrapolation capability on several datasets [25,26], performing exceptionally well even under high-temperature conditions [23].

Owing to these benefits, MACE has been extensively utilized in MD simulations, with our particular emphasis on its application within polymer systems. Poly(hexamethylene terephthalamide-co-isophthalamide) (noted as PA6T/6I) is a semi-aromatic polyamide known for its combination of the superior processing flowability characteristic of aliphatic polyamides, along with low water absorption, exceptional heat resistance, and notably enhanced mechanical properties [27,28]. The processing of PA6T/6I enables the development of a range of high-performance plastics and fibers. Consequently, conducting MD simulations on PA6T/6I to explore its thermodynamic properties is of considerable importance.

In this study, we compared the glass transition temperature (T_g) results obtained from simulations using the PCFF and the machine learning force field (MACE-OFF) against experimental values, thereby validating the precision of the MACE-OFF simulations. Moreover, we employed both methodologies to scrutinize the impact of varying PA6T contents and temperatures on the free volume, mean square displacement, and hydrogen bond numbers within the copolymer system. Ultimately, we delved into the correlation between the stacking pattern of the benzene rings and the number of hydrogen bonds. This research underscores the viability of employing MACE-based models in polymer dynamics simulations and illustrates that machine learning force fields can precisely elucidate the interplay between the structure and properties of materials.

2. Simulation models and computational details

2.1 Machine learning force fields

We utilized the MACE-OFF model, a short-range, transferable force field specifically designed for organic molecules and constructed on the foundation of the MACE model architecture [29]. This model is developed from first-principles reference data, which are generated using cutting-edge machine learning techniques [29]. It is parameterized for key chemical elements that are prevalent in organic chemistry, a feature that empowers the MACE-OFF model to precisely simulate neutral molecular systems, including drug molecules and biopolymers. MPNNs [30,31] represent a category of graph neural networks (GNNs) [32-35] that map a labeled graph to a target space, which can be either a graph or a vector space. The MPNN operates through a message passing mechanism between nodes, where, at each layer, a node's feature information is integrated with the features of its neighboring nodes. This process enables the model to learn a comprehensive representation of both the individual nodes and the graph as a whole.

Figure 1. Workflow of the MACE model.

The workflow of the MACE model is illustrated in Figure 1. MACE [22] is a machine learning architecture that takes the positions and chemical elements of atoms as input and learns to predict the potential energy of atomic systems. The total energy is decomposed into atomic site energies, enabling linear scaling with system size:

$$E_{total} = \sum_{i} E_i \tag{1}$$

Each atom and its environment are represented as a graph, where nodes correspond to atoms, and edges are defined for neighboring atoms within a cutoff distance r_{cut}. The initial node features are learnable embeddings of the atomic numbers:

$$h_{i,k00}^{(0)} = \sum_{z} W_{kz}\, \delta_{zz_i} \tag{2}$$

These features are updated through a message-passing process, which iteratively incorporates information from neighboring atoms and their geometric arrangement. At each layer t, atomic features are updated as:

$$h_{i,kLM}^{(t+1)} = \sum_{\bar{k}} W_{kL,\bar{k}}^{(t)}\, m_{i,\bar{k}LM}^{(t)} + \sum_{\bar{k}} W_{kz_iL,\bar{k}}^{(t)}\, h_{i,\bar{k}LM}^{(t)} \tag{3}$$

where $m_{I,\bar{k}LM}^{(t)}$ are messages constructed from equivariant many-body features of the local environment. In the first layer (t = 0), only the first term is present. After two iterations (layers), the site energy of each atom is obtained via read-out functions applied to the updated features:

$$E_i = \sum_{t=1}^{2} \mathcal{R}^{(t)}\left(\mathbf{h}_i^{(t)}\right), \tag{4}$$

With

$$\mathcal{R}^{(t)}\left(\mathbf{h}_i^{(t)}\right) = \begin{cases} \sum_k W_k^{(t)} h_{i,k00}^{(t)} & \text{for } t = 1 \\ \mathrm{MLP}\left(\left\{h_{i,k00}^{(t)}\right\}_k\right) & \text{for } t = 2 \end{cases} \tag{5}$$

The total force and stress are computed as analytical derivatives of the predicted total energy with respect to atomic positions and strain, respectively. Additional mathematical details and all intermediate equations are provided in the Supporting Information (SI, ESI†).

2.2 MD simulations of copolymers

The glass transition process can be explained by the free volume theory proposed by Fox and Flory [36-38], at lower temperatures, the change in the free volume of the polymer is very small, and a sudden change occurs at T_g, which is the temperature at which the free volume reaches a critical value. In this study, we employed two methods to analyze the density-temperature curves of PA6T/6I copolymers with different PA6T content based on this theory, thereby calculating their T_g. This has become a well-established method for studying the glass transition process of polymers. We constructed PA6T/6I copolymer systems with mass fractions of 45%, 50%, 55%, and 60% (denoted as P-45, P-50, P-55, and P-60, respectively) to systematically study the effects of temperature, PA6T content, and different computational methods on the thermal properties of the copolymer.

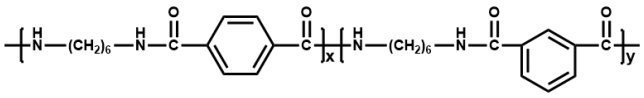

Figure 2. The structure of the PA6T/6I copolymer (where x = 9 and x = 11 represent the number of repeating units of PA6T in P-45 and P-55, respectively; x = 5 and x = 6 represent the number of repeating units of PA6T in P-50 and P-60, respectively). In P-45 and P-55, the number of repeating units of PA6I is given by y = 20 - x; in P-50 and P-60, the number of repeating units of PA6I is given by y = 10 - x.

The molecular structures of the PA6T/6I copolymers are shown in Figure 2, with each copolymer model consisting of five chains. Each chain in the P-45 and P-55 models contained 20 repeating units, while it contained 10 repeating units in the P-50 and P-60 models. To reduce potential human bias and guarantee the stability of the structure, the initial positions of the polymer chains were set randomly during the copolymer model construction. This randomization method effectively simulates the amorphous nature of the copolymers observed in experiments, thereby reducing any bias in the initial configurations. The polymer consistent force field (PCFF) [39] can simultaneously simulate both covalent bonding and non-covalent interactions in polymers, making it highly suitable for complex macromolecular systems. It has been widely used in studies of structural and dynamic properties of polymer materials [40,41], including polyamides and other polymers [42-44]. In this study, we utilized both the PCFF and the MACE-OFF machine learning model to perform MD simulations on four PA6T/6I models. In the simulations, both molecular and non-bonded interactions were accounted for, with van der Waals forces computed using the Lennard-Jones 9-6 potential and electrostatic interactions handled through the Coulombic contribution.

The simulations were carried out using the LAMMPS package (large-scale atomic/molecular massively parallel simulator) [45], with data visualization performed through OVITO software [46]. To solve the equations of motion, the Verlet algorithm [47] was employed with a timestep of 1 fs, and periodic boundary conditions were applied in all directions. Temperature and pressure were regulated using the Nosé–Hoover thermostat and the Barostat [48], respectively. A cutoff distance of 12 Å was set for the van der Waals interactions, and long-range electrostatic interactions were computed using the particle-particle, particle-pesh (PPPM) method [49], ensuring a precision of 10^{-6} to maintain result accuracy.

The initial molecular structures were energy minimized using the steepest descent method. As mentioned earlier, we ensured that the initial models were constructed with disorder to avoid any human-induced errors. To prevent any unreasonable local configurations in the initial model, the system was gradually heated from 260 K to 640 K under constant temperature and pressure (NPT) conditions. Once at 640 K, the system was held for 2 ns to relieve any residual stresses and optimize the local structure. Following this, the system was cooled from 640 K to 260 K at a rate of 9.5 K/ns. During each 20 K decrease in temperature, the system was equilibrated for 1 ns at the new temperature using NVT conditions, followed by a 3 ns NPT simulation, with the final 2 ns dedicated to data collection. Throughout the simulations, the pressure was kept constant at 0.1 MPa.

The MACE-OFF MD simulations were performed using the atomic simulation environment (ASE) [50], a Python-based package designed for setting up, guiding, and analyzing atomic-scale simulations. A timestep of 1 fs was used, with periodic boundary conditions applied in all directions. Temperature and pressure were controlled using the Nosé–Hoover thermostat and Barostat, respectively. To eliminate potential unreasonable local configurations in the initial model, we use the final frame of the NPT process under each cooling condition from the PCFF as the initial structure for the ASE dynamic simulation. This approach eliminates potential unreasonable local configurations in the initial model and significantly reduces the simulation time for the machine learning model's dynamics. The machine learning model is then applied to simulate a 1 ns dynamic process at each temperature point. For more details on the MACE-OFF simulations, please refer to the Supplementary Information (SI, ESI†).

We calculated the free volume fraction (FFV) using the atomic volume and surface module in Materials Studio [51], while the system's free volume was determined via the Connolly surface method, employing a hard sphere probe with a radius of 0.1 nm [52] . The rate of change in free volume shows significant differences near the T_g, primarily due to the different responses of free volume to temperature changes above and below T_g. To determine T_g, we performed linear fitting of the density data in the low and high-temperature regions, with the intersection of the lines corresponding to the system's T_g.

3. Results and discussion

In this study, we primarily employed the small-accuracy MACE-OFF model to perform MD simulations and subsequent property analyses. To further assess the impact of model accuracy on the dynamical results, MD simulations of the P-50 system were also

carried out using the medium- and large-accuracy MACE-OFF models. The corresponding results are provided in the Supporting Information (SI, ESI†). To accurately predict the thermal properties of PA6T/6I, we propose enhancing the reliability of conventional force fields (e.g., PCFF) by benchmarking the dynamic structures and derived properties from the machine learning force field, MACE-OFF, against experimental data. First, we performed force field calibration for PA6T/6I monomers, systematically evaluating the simulation accuracy of MACE-OFF, PCFF, and density functional theory with high-precision functionals. For copolymer systems with varying PA6T compositions, we further investigated the temperature dependence of hydrogen bonding and free volume fraction, as well as their influence on T_g. This section provides a comprehensive analysis of these factors across copolymer systems with different PA6T contents. During MD simulations, the copolymer system exhibits significant density variations upon cooling. This phenomenon arises from temperature-induced changes in polymer chain mobility, which directly affect the overall packing density of the simulated system.

3.1 Force field calibration

Previous studies have suggested that density functional theory(DFT) can provide an accurate description of both hydrogen bonding and π-π stacking interactions when supplemented with dispersion corrections [53-55]. To validate the accuracy of the PCFF and MACE-OFF force field parameters, we utilized a suite of highly precise computational approaches, encompassing the generalized energy-based fragmentation (GEBF) coupled with the coupled-cluster singles and doubles with perturbative triples (CCSD(T)) method, as well as the M06 and ωB97M-D3(BJ) density functionals. The GEBF-CCSD(T) method was executed with the aid of LSQC 3.0 software [56]. The GEBF technique stands out as an effective strategy for molecular fragmentation [57-59], predicated on the concept of segmenting a large molecule into smaller, manageable subsystems or fragments. The energies of these fragments are computed individually and then aggregated to compute the total energy of the molecule. In the fragmentation of PA6T, we strategically partitioned the benzene rings and amide groups into distinct segments and further divided the remaining atoms within the covalently bonded system into fragments, each incorporating 2 to 3 non-hydrogen atoms. This systematic approach is visually elucidated in Figure S1(ESI†). These methods are expected to provide a reasonable description of van der Waals interactions. The calibration results for poly(terephthaloyl hexylenediamine) (PA6T) monomer interactions are shown in Figure S2(ESI†). In the calibration of hydrogen bond interactions, GEBF-based CCSD(T) predicts a stable hydrogen bond length of 2.0 Å, while both PCFF and DFT (M06 and ωB97M-D3(BJ)) predict a stable hydrogen bond length of 1.9 Å. For π-π stacking interactions (Figure S2b, ESI†), all four methods predict an equilibrium stacking distance of 3.5 Å. Additionally, the M06 and GEBF-based CCSD(T) calculations yield a maximum energy deviation of less than 3.0 kcal/mol, while ωB97M-D3(BJ) and PCFF differ by approximately 5.0 and 7.0 kcal/mol, respectively. These results demonstrate that the M06 method provides a more accurate description of both hydrogen bonding and π-π stacking interactions. They also indicate that ωB97M-D3(BJ) retains a reasonable level of accuracy. Based on these findings, we selected the M06 and ωB97M-D3(BJ) functionals with the cc-pVDZ basis set to further validate the PCFF and MACE-OFF parameters for PA6T/6I copolymers. It should be noted that, for the force field calibration of the PA6T/6I system, all structures were generated via direct single-point energy calculations without geometry optimization. This approach was adopted to ensure that the inter-structural distances were strictly consistent with the predefined values.

The hydrogen bond interaction calibration, shown in Figure 3a, spans distances from 1.5 to 5.0 Å across different methods. The MACE-OFF model achieves accuracy comparable to M06, with an energy deviation of about 1.0 kcal/mol at larger separations (4.0-5.0 Å), defined as the O-H distance in amide groups. Both MACE-OFF and DFT (M06 and ωB97M-D3(BJ)) predict a stable hydrogen bond length of 2.1 Å, whereas PCFF yields a slightly longer bond (2.2 Å). This indicates that MACE-OFF better reproduces hydrogen bonding interactions, according to M06 method. However, compared to ωB97M-D3(BJ), both MACE-OFF and PCFF slightly underestimate hydrogen bond strength. Given the abundance of strong hydrogen bonds in PA6T/6I, the longer bond distance predicted by PCFF leads to looser chain packing, resulting in lower copolymer density, a factor that may compromise the accuracy of T_g predictions.

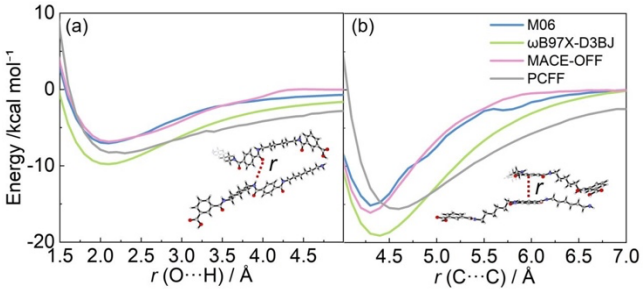

Figure 3. Calibration results for hydrogen-bonding interactions (a) and π-π stacking interactions (b). The M06 and ωB97M-D3(BJ) calculations are performed using the cc-pVDZ basis set in comparison with PCFF and MACE-OFF methods.

In the analysis of π-π stacking interactions (Figure 3b), the MACE-OFF model yields predictions closely aligned with the M06 method, consistent with its performance for hydrogen bonding. MACE-OFF achieves an equilibrium stacking distance of 4.3 Å, whereas PCFF predicts a longer distance (4.6 Å), leading to a looser packed conformation and significantly influencing the system's density during simulations. Compared to ωB97M-D3(BJ), PCFF underestimates π-π stacking interactions by about 14.0 kcal/mol, while showing closer agreement with M06. This substantial discrepancy in interaction energies further highlights the limitation of PCFF in accurately modeling the PA6T/6I copolymer system. We will compare both the packing arrangements and their derived thermal properties obtained from PCFF and MACE-OFF MD simulations.

3.2 Thermal properties of copolymers

The accuracy of the parameters in the force field can be validated through the thermal properties, such as the glass transition temperature (T_g) derived from the simulated microstructures. We compared the simulated T_g values with experimental observations [60], where T_g for PA6T/6I copolymers with varying PA6T content were obtained by fitting multiple experimental data points. The T_g of the polymer, determined through least squares fitting, is shown in Figure 4. The comparison of experimental measurements and simulated results is summarized in Table 1. We further compared the simulation results between PCFF and MACE-OFF, as illustrated in Figure 4. Although the trend in T_g variation is consistent with the

experimental results, the relative error between the PCFF simulation and experimental values is significant, indicating a need for more accurate predictions of T_g. Table 1 shows that MACE-OFF simulations provide an excellent agreement with the experimental values, with a relative error of approximately 1.0%. Specifically, as the PA6T content increases, the simulated T_g values of the copolymer also increase, which is consistent with the experimental trend. Drawing from experimental density measurements, the copolymer composed of 30 wt% PA6T and 70 wt% PA6I is reported to have a density of 1.185 g/cm^3 [61].With the increment of PA6T content, the density of the copolymer system experiences a modest increase as well [60]. To ascertain the average densities of polymer simulations across varying compositions at ambient temperature (298 K), we employed both force fields. The PCFF simulation produced a density of 1.132 g/cm^3, whereas the MACE-OFF simulation yielded a density of 1.219 g/cm^3. This indicates that the density obtained from the MACE-OFF simulation is closer to the experimental value, suggesting that it provides a better description of the microstructure. In summary, these results demonstrate that MACE-OFF is expected to describe the thermal properties more accurately than the traditional force field, such as PCFF.

Table 1. T_g results of P-45, P-50, P-55, and P-60 simulated using MACE-OFF and PCFF.

System	Experimental T_g (K)[60]	MACE-OFF (K)	Relative error (%)	PCFF (K)	Relative error (%)
P-45	397.8	400.7	0.7	375.2	5.7
P-50	398.2	402.5	1.1	410.1	3.0
P-55	/	416.1	/	415.7	/
P-60	/	417.8	/	481.1	/

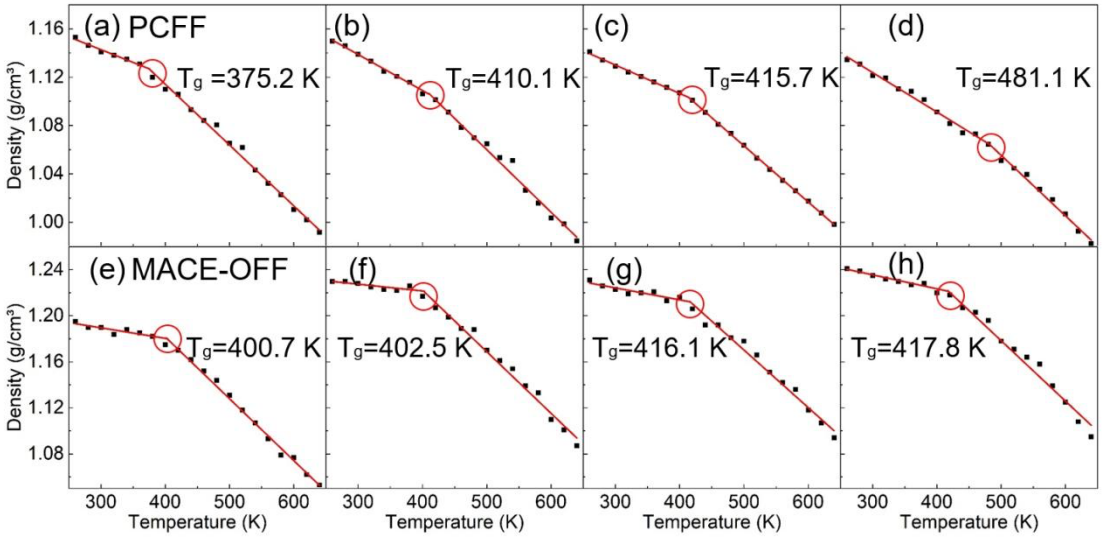

Figure 4. (a-d) Density-temperature curves for P-45, P-50, P-55, and P-60 simulated by PCFF, and (e-h) for the same compounds simulated by MACE-OFF. The red curves represent the fitted density data in the high and low temperature regions, with the intersection points marked as T_g.

Free volume is a critical concept used to describe the available space for molecular chain movement within materials and the ease with which these chains can flow. In polymer systems, free volume is typically manifested as spaces between polymer chains, often appearing as spherical or ellipsoidal voids [62-64]. These voids play a crucial role in polymer research, as they directly link the free volume to the glass transition temperature T_g of polymers [65], thereby providing a theoretical foundation for understanding the polymer glass transition process. As a result, analyzing free volume is essential for studying the thermodynamic properties of polymers.

Free volume refers to the space within the entire system in which molecules can move freely. The total volume (V_t) of the system can be considered as the sum of the void volume and the occupied volume (V_o), where the occupied volume can be calculated by summing the free volume contributions of each atom [66]. The fractional free volume (FFV) is defined as :

$$FFV = \frac{V_t - V_o}{V_t} \quad (6)$$

In this study, V_o is calculated using a hard-sphere probe technique. This technique involves rolling a sphere with a radius of 1 Å across the surface of the polymer. Once the scanning process is completed, the molecules are enclosed by a surface, and the volume enclosed within this surface is considered as V_o.

Figure S3(a) (ESI†) displays a snapshot of the free volume within the P-45 equilibrium structure as simulated using the PCFF force field. The van der Waals surface delineates the volume occupied by the polymer, whereas the Connolly surface outlines the free volume available.[67] Furthermore, the variation of free volume

with temperature for copolymer systems with different PA6T contents is illustrated in Figure S3(b) (ESI†), also simulated using the PCFF. As it shows, below 460 K, the free volume of the copolymer system increases slowly. However, above 460 K, the increase becomes more pronounced. It demonstrates that atomic positions are almost stable at lower temperatures, and the movement of chain segments is sluggish, resulting in minimal changes in the free volume of the system. In contrast, as the temperature increases beyond a certain threshold, thermal energy enhances the mobility of the chain segments. This increased mobility leads to a significant expansion of the space between the chains, resulting in greater molecular motion within the system and a rapid increase in the free volume.

We present snapshots of the free volume when simulating the P-45 equilibrium structure using the MACE-OFF model in Figure 5, along with the trend of free volume variation with temperature in the copolymer system. As the temperature increases, the free volume of the system gradually rises, a trend consistent with the results obtained from the PCFF simulation (Figure S3(b) (ESI†)). However, at the same temperature, the fractional free volume (FFV) values derived from the MACE-OFF simulation are consistently lower than those from the PCFF simulation. This observation aligns with our previous finding that the density of the system simulated using MACE-OFF is higher than that simulated using PCFF. These results further confirm the positive correlation between free volume and temperature. Additionally, they provide insights into the relationship between free volume and system density. By elucidating these connections, our study offers a theoretical foundation for understanding the thermodynamic properties of the PA6T/6I copolymer and deepens the understanding of the relationship between microstructural changes and free volume.

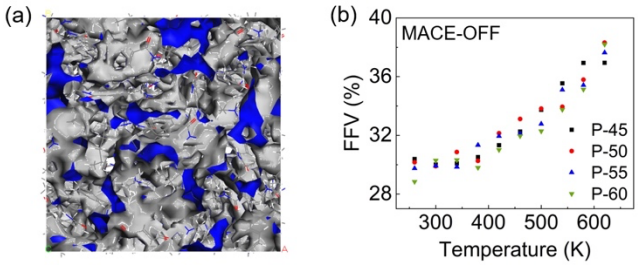

Figure 5. (a) Snapshot of P-45 simulated with MACE-OFF at T=298.15 K, with the van der Waals surface in gray and Connolly surface in blue. (b) FFV values of P-45, P-50, P-55, and P-60 at different temperatures, simulated by MACE-OFF, with solid black squares, red circles, blue triangles, and green inverted triangles, respectively.

The mean squared displacement (MSD) is a powerful tool for studying the diffusion properties of polymer segments, thereby providing insights into their dynamic behavior. It quantifies the average squared distance that polymer chain segments or the center of mass of the polymer chain travel over time. The slope of the MSD curve is directly related to the mobility of the polymer segments [68], and it is calculated as follows:

$$MSD(t) = \left\langle \left(\mathrm{X}_i(t) - \mathrm{X}_i(0) \right)^2 \right\rangle \qquad (7)$$

where, $\mathrm{X}_i(t)$ and $\mathrm{X}_i(0)$ represent the position of atom *i* at time *t* and at the initial time t = 0, respectively. Figure 6 illustrates the variation of the MSD for PA6T/6I copolymers with different PA6T/6I ratios, simulated using both PCFF and MACE-OFF, over a temperature range from 260 K to 640 K.

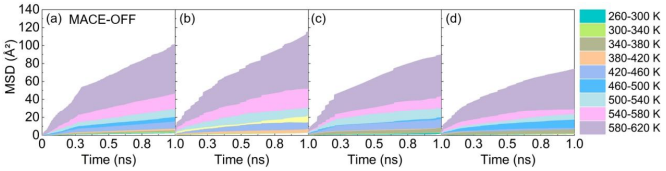

Figure 6. MSD curves for P-45(a), P-50(b), P-55(c), and P-60(d) simulated with MACE-OFF.

The mean squared displacement results for the copolymer simulated using PCFF and MACE-OFF are presented in Figure S4(ESI†) and Figure 6, respectively. Both simulation methods indicate that MSD increases over time, with a more pronounced increase observed at higher temperatures. This trend is attributed to the increased thermal energy available at higher temperatures, which enhances the mobility of atoms and polymer chains. Comparing the results from both simulation methods reveals that, at the same temperature, the MSD in the MACE-OFF simulated system is significantly smaller than that in the PCFF simulation. This observation can be explained by the force field calibration results, which show that the minimum energy points in the MACE-OFF system are located closer together. The stronger π-π interactions between polymer chains at these shorter distances more effectively restrict chain motion, resulting in smaller MSD values.

Additionally, the MSD of the system undergoes significant changes within a specific temperature range due to the glass transition process in polymers. Specifically, when the temperature exceeds the glass transition temperature, the increase in MSD becomes much more pronounced compared to temperatures below T_g, indicating a shift in the atomic movement pattern. Experimentally, T_g of the PA6T/6I copolymer is around 400 K.[61] According to the PCFF simulation results (Figure S4(ESI†)), the MSD experiences a sharp increase in the 380-420 K range for P-45, P-50, and P-60, while for P-55, the increase occurs in the 340-380 K range. The MACE-OFF simulation results show a similar trend, with MSD increasing sharply in the 380-420 K range for P-45 and P-50, and in the 340-380 K range for P-55 and P-60. This phenomenon suggests that both PCFF and MACE-OFF simulations can predict the approximate range of the T_g for the PA6T/6I copolymer, although with some deviation. Overall, these MSD studies indicate that the atomic motion undergoes significant changes before and after the glass transition in polymers. This finding provides important insights for further investigating the relationship between polymer structural changes and temperature.

3.3 Hydrogen bonding in copolymers

Hydrogen bonds are instrumental in stabilizing the static structure of polymers and in modulating their dynamic properties. Recognized as the most potent intermolecular interaction subsequent to chemical bonds, the examination of hydrogen bonds is of paramount importance. Their influence on material properties is profound, for instance, they can bolster the thermal and mechanical attributes of materials. In the PA6T/6I copolymer system, hydrogen bonds are established through the interactions between hydrogen and oxygen atoms within the amide bonds. This study delves into the variations in the distance and angle of the N–H···O hydrogen bonds within the copolymer. The schematic representations of both inter-chain and

intra-chain hydrogen bonds are depicted in Figure 7a. A hydrogen bond is deemed to be formed when the N···O distance is less than 3.5 Å and the N-H···O angle surpasses 160°. Given that the number of amide groups fluctuates across copolymer systems with varying PA6T contents, revealing the total hydrogen bonds in each system falls short for a thorough analysis. Consequently, we normalize the number of hydrogen bonds formed at different temperatures relative to the number of PA6T and PA6I monomers present in each system, that is, by calculating the average number of hydrogen bonds per monomer. This normalization allows us to more accurately analyze the trends in hydrogen bond quantities across systems with different PA6T contents.

Moving forward, we computed the average number of hydrogen bonds per monomer for both inter-chain and intra-chain interactions across all copolymer systems at 400 K. The selection of 400 K is predicated on the experimentally ascertained glass transition temperature of PA6T/6I. As illustrated in Figures 7b-c, which present the hydrogen bond counts (HBs), inter-chain hydrogen bonds (inter-chain HBs), and intra-chain hydrogen bonds (intra-chain HBs), it becomes evident that inter-chain hydrogen bonds predominantly govern the hydrogen bonding interactions and significantly affect the magnitude of T_g. Inter-molecular hydrogen bonds enhance the intermolecular interactions, thereby potentially elevating the T_g. In contrast, hydrogen bonds within the molecular chain diminish the system's rigidity, consequently lowering the T_g. With increasing PA6T content, the number of inter-chain hydrogen bonds in the copolymer systems at 400 K rises progressively, a trend that aligns with the observed changes in T_g.

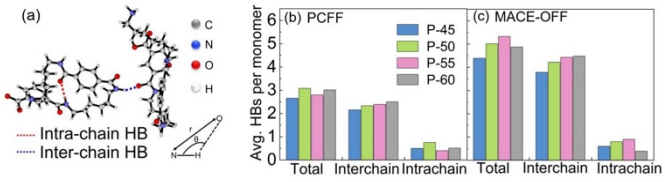

Figure 7. (a) A schematic diagram illustrates the inter-chain and intra-chain hydrogen bonds as observed from the equilibrium trajectory simulations. The total number of hydrogen bonds (HBs), which includes both intra-chain and inter-chain components, is presented for the P-45, P-50, P-55, and P-60 copolymer systems, all of which were simulated using the PCFF (b) and MACE-OFF (c).

As depicted in Figures 8a-b, the number of hydrogen bonds in all systems modeled with both PCFF and MACE-OFF force fields gradually diminishes with rising temperature. This trend can be attributed to the increased mobility of polymer chain segments and the enhanced thermal energy provided to the system at higher temperatures. These factors collectively contribute to an increase in the inter-chain distance, which in turn leads to a progressive decrease in hydrogen bonding. Upon examining Figure 8a, it is evident that within the low-temperature regime of the PCFF-simulated systems, the P-50 system exhibits a higher count of hydrogen bonds compared to the other systems. As temperature continues to rise, the hydrogen bond count across all four systems tends to level off. Figure 8b reveals that in the MACE-OFF-simulated systems, the hydrogen bond count escalates with increasing PA6T content at lower temperatures. Furthermore, as the temperature ascends, the hydrogen bond count across the systems begins to converge. To delve deeper into the influence of polymer conformational changes on thermal properties and to elucidate the mechanism behind the variation in hydrogen bond numbers with increasing PA6T content, we conducted an analysis of the stacking patterns of aromatic rings within different PA6T/6I copolymers.

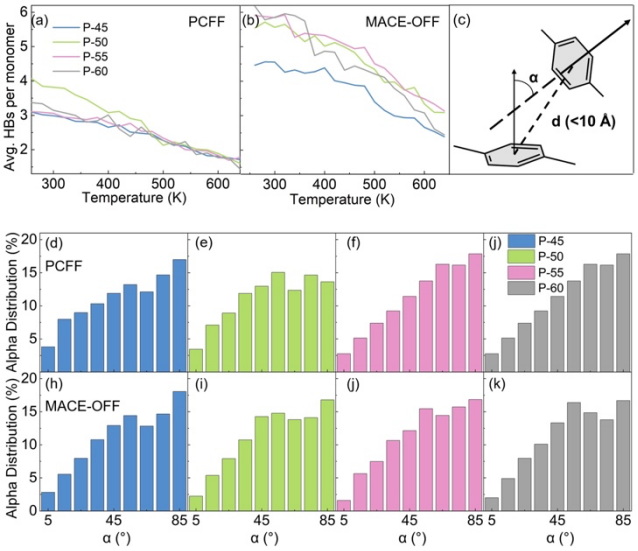

Figure 8. (a) Average number of hydrogen bonds per monomer for P-45, P-50, P-55, and P-60 in the PCFF (a) and MACE-OFF simulations (b). (c) Schematic diagram of benzene ring stacking angles and distances. Angle α between the normal vectors of two benzene rings with a center-to-center distance of 10 Å in the PA6T/6I system simulated with PCFF (d-g) and MACE-OFF simulations (h-k).

Given the substantial alterations in polymer segment motion around the glass transition temperature, we scrutinized the distribution of stacking angles between benzene rings in each system prior to reaching the experimental T_g value of 400 K. Our objective was to uncover the correlation between the system's hydrogen bond count and the benzene ring angles. Our analysis was further nuanced by focusing on aromatic ring stacking arrangements with inter-ring distances of less than 10 Å. Figures 8d-k illustrate the relative orientation distribution (α) of aromatic rings across various polymer chains. When the stacking angle of the aromatic rings approaches 90°, the steric hindrance between the rings intensifies, promoting a T-shaped configuration over the more favorable π-π stacking. This configuration impedes hydrogen bond formation, leading to a reduction in their quantity. In the PCFF simulation outcomes, the P-50 system has the smallest number of aromatic ring pairs with angles ranging from 80° to 90°, and thus, it displays the highest number of hydrogen bonds when compared to the other three systems. Conversely, in the MACE-OFF simulation outcomes, P-50, P-55, and P-60 systems have fewer aromatic ring pairs with angles between 80° and 90° than the P-45 system, which results in these three systems exhibiting a higher number of hydrogen bonds than the P-45 system.

3.4. Ab tnitio trained machine learning force fields based on MACE

MACE-OFF-Small has demonstrated accuracy in predicting conformational energies, torsional potential energy surfaces, structural optimizations, and physical properties in organic

molecules, achieving a mean absolute error of 1.20 meV/atom for energy and 29.51 meV/Å for forces on its reported test datasets.

Nevertheless, several challenges remain when applying the MACE-OFF model to molecular dynamics simulations of polymers. The model does not sufficiently account for long-range interactions between polymer chains, and its training set does not incorporate configurations, energetic, and force information specific to particular polymer systems. As a result, the model exhibits certain limitations in describing system-specific structure–property relationships, which restricts its generalizability and predictive accuracy for complex polymeric materials. To address these issues, a feasible strategy is to construct a high-quality dataset tailored to the target polyamide structure (in this study, PA6T/6I), and to train a machine learning force field specifically adapted to polyamide systems. The detailed procedure for dataset construction is presented in the Supporting Information (SI, ESI†).

This comprehensive data generation workflow ensures that the resulting training set encompasses the structural diversity and relevant chemical environments present in polyamide systems, thereby providing a solid foundation for the development of accurate and transferable machine learning force fields. Although the initial model performance is not yet fully satisfactory, the established data pipeline facilitates further optimization and benchmarking. Detailed parameter settings and model evaluation results are also provided in the Supporting Information (SI, ESI†).

However, despite these efforts, the mean absolute errors (MAEs) of energy and force for our trained model are 7.4 eV and 8.7 eV/Å, respectively. Such high errors reflect insufficient accuracy in describing the energies and forces of molecular structures, which weakens the model's ability to provide reliable structural and property predictions. Therefore, further hyperparameter optimization is necessary to lower these errors and enhance model accuracy. In addition, expanding the dataset—particularly by incorporating structures containing benzene rings and amide groups—would further improve the model's predictive capabilities. This would enable the ab initio-trained model to more accurately predict key properties of polyamide and related amide-containing polymers, including thermodynamic properties (such as glass transition temperature and melting point), mechanical performance, and microstructural evolution.

4. Conclusion

In this research, we conducted a comparative analysis of the glass transition temperature (T_g) of PA6T/6I copolymers with varying PA6T content, utilizing both the PCFF and MACE-OFF models. The calibration of the force fields revealed that the MACE-OFF model closely aligns with the M06 functional in characterizing hydrogen-bonding and π-π stacking interactions among the copolymers. When contrasted with PCFF simulations, the MACE-OFF model yields a T_g value that is derived from the density-temperature equilibrium curve and is in good accord with experimental observations. Thermodynamic analyses, grounded in free volume and mean squared displacement, unveiled the patterns of chain segment mobility as a function of temperature. Subsequent examinations of both inter-chain and intra-chain hydrogen bonds indicated that inter-chain hydrogen bonds are predominant in hydrogen bonding interactions, and there is a notable increase in T_g with an increase in the number of inter-chain hydrogen bonds. Ultimately, the study of the relationship between the stacking arrangement of benzene rings and the number of hydrogen bonds revealed that an increase in the number of benzene rings with angles between 80° and 90° leads to a T-shaped configuration, which is detrimental to the formation of hydrogen bonds. This investigation offers an exhaustive exploration of the thermal properties of PA6T/6I copolymers at the molecular level and underscores the high precision of machine learning-based force fields in forecasting polymer characteristics through MD simulations.

Acknowledgments

This work was supported by the National Key Research and Development Program of China (2023YFB3712500), AI-Enhanced Research Program of Shanghai Municipal Education Commission (SMEC-AI-DHUY-06), and the Fundamental Research Funds for the Central Universities (2232023A-02).

Supporting Information

The online version contains supplementary material available at website https://global-sci.com/storage/self-storage/cicc-2025-120-1-r1-si.pdf

References

[1] Marx D. and Hutter J., Ab initio molecular dynamics: theory and implementation. *Mod. Methods Quantum Chem.*, **1** (2000), 141.

[2] Tuckerman M.E., Ab initio molecular dynamics: basic concepts, current trends and novel applications. *J. Phys.: Condens. Matter*, **14** (2002), R1297.

[3] Parr R.G., Electron Distributions and the Chemical Bond, Springer, (1982), 95–100.

[4] Cohen A.J., Mori-Sánchez P. and Yang W., Challenges for density functional theory. *Chem. Rev.*, **112** (2012), 289–320.

[5] Verma P. and Truhlar D.G., Status and challenges of density functional theory. *Trends Chem.*, **2** (2020), 302–318.

[6] Karplus M. and McCammon J.A., Molecular dynamics simulations of biomolecules. *Nat. Struct. Biol.*, **9** (2002), 646–652.

[7] Monticelli L. and Tieleman D.P., Force fields for classical molecular dynamics. *Methods Mol. Biol.*, (2013), 197–213.

[8] Sumpter B.G., Getino C. and Noid D.W., Theory and applications of neural computing in chemical science. *Annu. Rev. Phys. Chem.*, **45** (1994), 439–481.

[9] Jiang B., Li J. and Guo H., Potential energy surfaces from high fidelity fitting of ab initio points: the permutation invariant polynomial–neural network approach. *Int. Rev. Phys. Chem.*, **35** (2016), 479–506.

[10] Deringer V.L., Caro M.A. and Csa´nyi G., Machine learning interatomic potentials as emerging tools for materials science. *Adv. Mater.*, **31** (2019), 1902765.

[11] Vasudevan R., Pilania G. and Balachandran P.V., Machine learning for materials design and discovery. *J. Appl. Phys.*, **129** (2021).

[12] Yu Q., Ma R., Qu C., Conte R., Nandi A., Pandey P., Houston P.L., Zhang D.H. and Bowman J.M., Extending atomic decomposition and many-body representation with a chemistry-motivated approach to machine learning potentials. *Nat. Comput. Sci.*, (2025), 1–9.

[13] Schu¨tt K.T., Chmiela S., Von Lilienfeld O.A., Tkatchenko A., Tsuda K. and Mu¨ller K.-R., Machine learning meets quantum physics. *Lect. Notes Phys.*, (2020).

[14] Svozil D., Kvasnicka V. and Pospichal J., Introduction to multi-layer feed-forward neural networks. *Lab. Autom. Inf. Manage.*, **39** (1997), 43–62.

[15] Teso-Fz-Betoño A., Zulueta E., Cabezas-Olivenza M., Teso-Fz-Betoño D. and Fernandez-Gamiz U., A study of learning issues in feedforward neural networks. *Mathematics*, **10** (2022), 3206.

[16] Behler J. and Parrinello M., Generalized neural-network representation of high-dimensional potential-energy surfaces. *Phys. Rev. Lett.*, **98** (2007), 146401.

[17] Vassilev-Galindo V., Fonseca G., Poltavsky I. and Tkatchenko A., Challenges for machine learning force fields in reproducing potential energy surfaces of flexible molecules. *J. Chem. Phys.*, **154** (2021).

[18] Geiger M. and Smidt T., e3nn: Euclidean neural networks. *arXiv*, (2022), arXiv:2207.09453.

[19] Gilmer J., Schoenholz S.S., Riley P.F., Vinyals O. and Dahl G.E., Neural message passing for quantum chemistry. *International Conference on Machine Learning*, (2017).

[20] Xue L.-Y., Guo F., Wen Y.-S., Feng S.-Q., Huang X.-N., Guo L., Li H.-S., Cui S.-X., Zhang G.-Q. and Wang Q.-L., ReaxFF-MPNN machine learning potential: a combination of reactive force field and message passing neural networks. *Phys. Chem. Chem. Phys.*, **23** (2021), 19457–19464.

[21] Pozdnyakov S.N. and Ceriotti M., Incompleteness of graph neural networks for points clouds in three dimensions. *Mach. Learn.: Sci. Technol.*, **3** (2022), 045020.

[22] Batatia I., Kovacs D.P., Simm G., Ortner C. and Csa´nyi G., MACE: higher order equivariant message passing neural networks for fast and accurate force fields. *Adv. Neural Inf. Process. Syst.*, **35** (2022), 11423–11436.

[23] Grunert M., Großmann M., Hanseroth J., Flototto A., Oumard J., Wolf J.L., Runge E. and Dreßler C., Modeling complex proton transport phenomena—exploring the limits of fine-tuning and transferability of foundational machine-learned force fields. *J. Phys. Chem. C*, (2025).

[24] Gelzinyte E., Oeren M., Segall M.D. and Cs´anyi G., Transferable machine learning interatomic potential for bond dissociation energy prediction of drug-like molecules. *J. Chem. Theory Comput.*, **20** (2023), 164–177.

[25] Kovács D.P., Oord C. v. d., Kucera J., Allen A.E., Cole D.J., Ortner C. and Csányi G., Linear atomic cluster expansion force fields for organic molecules: beyond RMSE. *J. Chem. Theory Comput.*, **17** (2021), 7696–7711.

[26] Batatia I., Batzner S., Kovács D.P., Musaelian A., Simm G.N., Drautz R., Ortner C., Kozinsky B. and Csányi G., The design space of E(3)-equivariant atom-centered interatomic potentials. *Nat. Mach. Intell.*, **7** (2025), 56–67.

[27] Salomone J.C. and Rice W.C., Positron annihilation spectroscopy. *Encyclopedia of Polymer Science and Engineering*, Edited by H.F. Mark, N.M. Bikales, C.G. Overberger and C.G. Menges, Wiley, New York, (1987), 514.

[28] Nielinger W., Brassat B. and Neuray D., Amorphe polyamide auf basis isophthalsäure und hexamethylendiamin. *Angew. Makromol.*, **98** (1981), 225–236.

[29] Kovács D.P., Moore J.H., Browning N.J., Batatia I., Horton J.T., Pu Y., Kapil V., Witt W.C., Magdau I.-B., Cole D.J., et al., MACE-OFF: short-range transferable machine learning force fields for organic molecules. *J. Am. Chem. Soc.*, (2025).

[30] Gilmer J., Schoenholz S.S., Riley P.F., Vinyals O. and Dahl G.E., Neural message passing for quantum chemistry. *International Conference on Machine Learning*, (2017), 1263–1272.

[31] Bronstein M.M., Bruna J., Cohen T. and Veličković P., Geometric deep learning: grids, groups, graphs, geodesics, and gauges. *arXiv*, (2021), arXiv:2104.13478.

[32] Scarselli F., Gori M., Tsoi A.C., Hagenbuchner M. and Monfardini G., The graph neural network model. *IEEE Trans. Neural Netw.*, **20** (2008), 61–80.

[33] Zhou R., Gao W., Xia L., Wu H. and Guo S., The study of damping property and mechanism of thermoplastic polyurethane/phenolic resin through a combined experiment and molecular dynamics simulation. *J. Mater. Sci.*, **53** (2018), 9350–9362.

[34] Battaglia P.W., Hamrick J.B., Bapst V., Sanchez-Gonzalez A., Zambaldi V., Malinowski M., Tacchetti A., Raposo D., Santoro A., Faulkner R., et al., Relational inductive biases, deep learning, and graph networks. *arXiv*, (2018), arXiv:1806.01261.

[35] Kipf T.N. and Welling M., Semi-supervised classification with graph convolutional networks. *arXiv*, (2016), arXiv:1609.02907.

[36] Fox Jr T.G. and Flory P.J., Second-order transition temperatures and related properties of polystyrene. I. Influence of molecular weight. *J. Appl. Phys.*, **21** (1950), 581–591.

[37] Fox Jr T.G. and Flory P.J., Further studies on the melt viscosity of polyisobutylene. *J. Phys. Chem.*, **55** (1951), 221–234.

[38] Fox T.G. and Flory P.J., The glass temperature and related properties of polystyrene. Influence of molecular weight. *J. Polym. Sci.*, **14** (1954), 315–319.

[39] Sun H., Mumby S.J., Maple J.R. and Hagler A.T., An ab initio CFF93 all-atom force field for polycarbonates. *J. Am. Chem. Soc.*, **116** (1994), 2978–2987.

[40] Singh A. and Kumar D., Effect of temperature on elastic properties of CNT–polyethylene nanocomposite and its interface using MD simulations. *J. Mol. Model.*, **24** (2018), 1–11.

[41] Zhang Y., Yang H., Sun Y., Zheng X. and Guo Y., Molecular dynamics simulations of mechanical properties of epoxy–amine: cross-linker type and degree of conversion effects. *Chin. Phys. B*, **31** (2022), 064209.

[42] Yeh I.-C., Rinderspacher B.C., Andzelm J.W., Cureton L.T. and La Scala J., Computational study of thermal and mechanical properties of nylons and bio-based furan polyamides. *Polymer*, **55** (2014), 166–174.

[43] Saidakhmetov P., Piyanzina I., Baiman G., Nedopekin O. and Tayurskii D., The glass transition temperature investigation of polymers by molecular dynamic simulations. *Bull. Karaganda Univ., Phys. Ser.*, **112** (2023), 57–64.

[44] Ma R., Huang D., Zhang T. and Luo T., Determining influential descriptors for polymer chain conformation based on empirical force-fields and molecular dynamics simulations. *Chem. Phys. Lett.*, **704** (2018), 49–54.

[45] Thompson A.P., Aktulga H.M., Berger R., Bolintineanu D.S., Brown W.M., Crozier P.S., In't Veld P.J., Kohlmeyer A., Moore S.G., Nguyen T.D., et al., LAMMPS—A flexible simulation tool for particle-based materials modeling at the atomic, meso, and continuum scales. *Comput. Phys. Commun.*, **271** (2022), 108171.

[46] Stukowski A., Visualization and analysis of atomistic simulation data with OVITO—the Open Visualization Tool. *Modell. Simul. Mater. Sci. Eng.*, **18** (2009), 015012.
[47] Verlet L., Computer experiments on classical fluids. I. Thermodynamical properties of Lennard-Jones molecules. *Phys. Rev.*, **159** (1967), 98.
[48] Evans D.J. and Holian B.L., The Nose–Hoover thermostat. *J. Chem. Phys.*, **83** (1985), 4069–4074.
[49] Buneman O., Computer Simulation Using Particles. (1983).
[50] Larsen A.H., Mortensen J.J., Blomqvist J., Castelli I.E., Christensen R., Dulak M., Friis J., Groves M.N., Hammer B., Hargus C., et al., The Atomic Simulation Environment—a Python library for working with atoms. *J. Phys.: Condens. Matter*, **29** (2017), 273002.
[51] Accelrys Software Inc., Materials Studio Modeling Environment, Release 6.0, Accelrys Software Inc., San Diego, 2011.
[52] Wang Y., Huo X., Yue S., Xu D., Zhang L., Wang X. and Yang M., Effect of incorporated amide blocks on the glass transition in polyesteramides. *Mater. Today Commun.*, **39** (2024), 109062.
[53] Tsuneda T. and Taketsugu T., Charge-transfer excitations. *π-Stacked Polymers and Molecules*, Edited by T. Nakano, Springer Japan, (2014), 245–270.
[54] Arey J.S., Aeberhard P.C., Lin I.-C. and Rothlisberger U., Hydrogen bonding described using dispersion-corrected density functional theory. *J. Phys. Chem. B*, **113** (2009), 4726–4732.
[55] Zhu Y., Alqahtani S. and Hu X., An assessment of dispersion-corrected DFT methods for modeling nonbonded interactions in protein kinase inhibitor complexes. *Molecules*, **29** (2024), 304.
[56] Li S., et al., LSQC Program, Version 3.0. (2025).
[57] Li W., Dong H., Ma J. and Li S., Structures and spectroscopic properties of large molecules and condensed-phase systems predicted by generalized energy-based fragmentation approach. *Acc. Chem. Res.*, **54** (2020), 169–181.
[58] Li S., Li W. and Ma J., Generalized energy-based fragmentation approach and its applications to macromolecules and molecular aggregates. *Acc. Chem. Res.*, **47** (2014), 2712–2720.
[59] Li S., Li W. and Fang T., An efficient fragment-based approach for predicting the ground-state energies and structures of large molecules. *J. Am. Chem. Soc.*, **127** (2005), 7215–7226.
[60] Cousin T., Galy J. and Dupuy J., Molecular modelling of polyphthalamides thermal properties: comparison between modelling and experimental results. *Polymer*, **53** (2012), 3203–3210.
[61] Endo M., Morishima Y., Yano S., Tadano K., Murata Y. and Tsunashima K., Miscibility in binary blends of aromatic and alicyclic polyamides. *J. Appl. Polym. Sci.*, **101** (2006), 3971–3978.
[62] Aramoon A., Breitzman T.D., Woodward C. and El-Awady J.A., Correlating free-volume hole distribution to the glass transition temperature of epoxy polymers. *J. Phys. Chem. B*, **121** (2017), 8399–8407.
[63] Wang S., Wang C. and Wang B., Microstructure and mechanical properties of polymers studied by positron annihilation. *J. Radioanal. Nucl. Chem.*, **210** (1996), 407–421.
[64] Jean A.C., Positron annihilation spectroscopy for chemical analysis: a novel probe for microstructural analysis of polymers. *Microchem. J.*, **42** (1990), 72–102.
[65] Wang X., Liu Y., Lu H. and Fu Y.-Q., On the free-volume model of multi-shape memory effect in amorphous polymer. *Smart Mater. Struct.*, **28** (2019), 125012.
[66] Bondi A., Van der Waals volumes and radii. *J. Phys. Chem.*, **68** (1964), 441–451.
[67] Connolly M.L., Analytical molecular surface calculation. *J. Appl. Crystallogr.*, **16** (1983), 548–567.
[68] Saha S. and Bhowmick A.K., An insight into molecular structure and properties of flexible amorphous polymers: a molecular dynamics simulation approach. *J. Appl. Polym. Sci.*, **136** (2019), 47457.